ESC-TR-2004-087

Project Report
NG-3

Wideband Aperture Coherence Processing for Next Generation Radar (NexGen)

K.M. Cuomo
S.D. Coutts
J.C. McHarg
N.B. Pulsone
F.C. Robey

30 July 2004

Lincoln Laboratory
MASSACHUSETTS INSTITUTE OF TECHNOLOGY
LEXINGTON, MASSACHUSETTS

Prepared for the Missile Defense Agency under Air Force Contract F19628-00-C-0002.

Approved for public release; distribution is unlimited.

This report is based on studies performed at Lincoln Laboratory, a center for research operated by Massachusetts Institute of Technology. This work was sponsored by the Missile Defense Agency under Air Force Contract F19628-00-C-0002.

This report may be reproduced to satisfy needs of U.S. Government agencies.

The ESC Public Affairs Office has reviewed this report, and it is releasable to the National Technical Information Service, where it will be available to the general public, including foreign nationals.

This technical report has been reviewed and is approved for publication.

FOR THE COMMANDER

Gary Tutungian
Administrative Contracting Officer
Plans and Programs Directorate
Contracted Support Management

Non-Lincoln Recipients

PLEASE DO NOT RETURN
Permission has been granted by the Contracting Officer to destroy this document, when it is no longer needed.

Massachusetts Institute of Technology
Lincoln Laboratory

Wideband Aperture Coherence Processing for Next Generation Radar (NexGen)

K.M. Cuomo
Group 34

S.D. Coutts
J.C. McHarg
F.C. Robey
Group 33

N.B. Pulsone
Kwajalein

Project Report NG-3

30 July 2004

Prepared for the Missile Defense Agency under Air Force Contract F19628-00-C-0002.

Approved for public release; distribution is unlimited.

Lexington Massachusetts

ABSTRACT

This report develops robust signal processing architectures and algorithms specifically designed to achieve multi-aperture coherence on transmit and receive. A key feature of our approach is the use of orthogonal radar waveforms that allow the monostatic and bistatic target returns to be separated at each receiver's matched filter output. By analyzing these returns, we may determine the appropriate transmit times and phases in order to cohere the various radar apertures using both narrowband and wideband waveforms. This process increases the array gain on receive to N^2 instead of N for the single transmitter case. Furthermore, when full coherence on transmit is achieved, the array gain is N^3. The performance of our coherence algorithms is quantified using Monte Carlo simulations and compared to the Cramer-Rao lower bound. A computational complexity study shows that our aperture coherence algorithms are suitable for a real-time implementation on an SGI Origin 3000 multi-processor computer.

TABLE OF CONTENTS

LIST OF ILLUSTRATIONS

LIST OF ILLUSTRATIONS
(Continued)

LIST OF TABLES

1. INTRODUCTION & MOTIVATION

Today's wideband radar systems have significantly increased the capability of ballistic missile defense systems to carry out real-time discrimination and target identification. This capability is primarily the result of improved target resolution and the development of advanced signal processing algorithms [1-4].

There is considerable interest within the Ballistic Missile Defense (BMD) community to develop transportable wideband radars that can be placed within, say, a few hundred yards of each other and used together in a coherent and cooperative way to significant improve target detection and discrimination capabilities. A system that can be moved and re-deployed within a reasonably short amount of time to meet a new or emerging threat is well-suited to today's ballistic missile defense environment. Distributed wideband radar apertures can be exploited in several beneficial ways: (i) the power-aperture-gain product of N coherent radar apertures is proportional to N^3; (ii) clutter or other forms of electronic countermeasures can be more effectively mitigated; (iii) adverse atmospheric effects can be minimized due to decorrelation and averaging over multiple distributed radar apertures; and (iv) detection and discrimination at low elevation angles can be significantly improved.

The Missile Defense Agency (MDA) recently sponsored a study [5] with researchers from laboratories, contractors and government agencies to investigate advanced radar sensor concepts that could meet the requirements of future ballistic missile threats. This study considered options that were previously restricted by the anti-ballistic missile treaty. One of the recommendations from this study is the development of a Next Generation Radar (NGR) system. The key capabilities of this new radar are: a transportable system, a flexible operating capability, improved discrimination capability, and an extensible design to meet evolving threats.

The mutually coherent operation of two or more wideband radars is a challenging task. The conceptual architecture for accomplishing this task is illustrated in Figure 1. In this figure, we assume connectivity from each sensor to a central operations center utilizing a medium to high bandwidth data link capable of communicating multiple pulse amplitude and phase data.

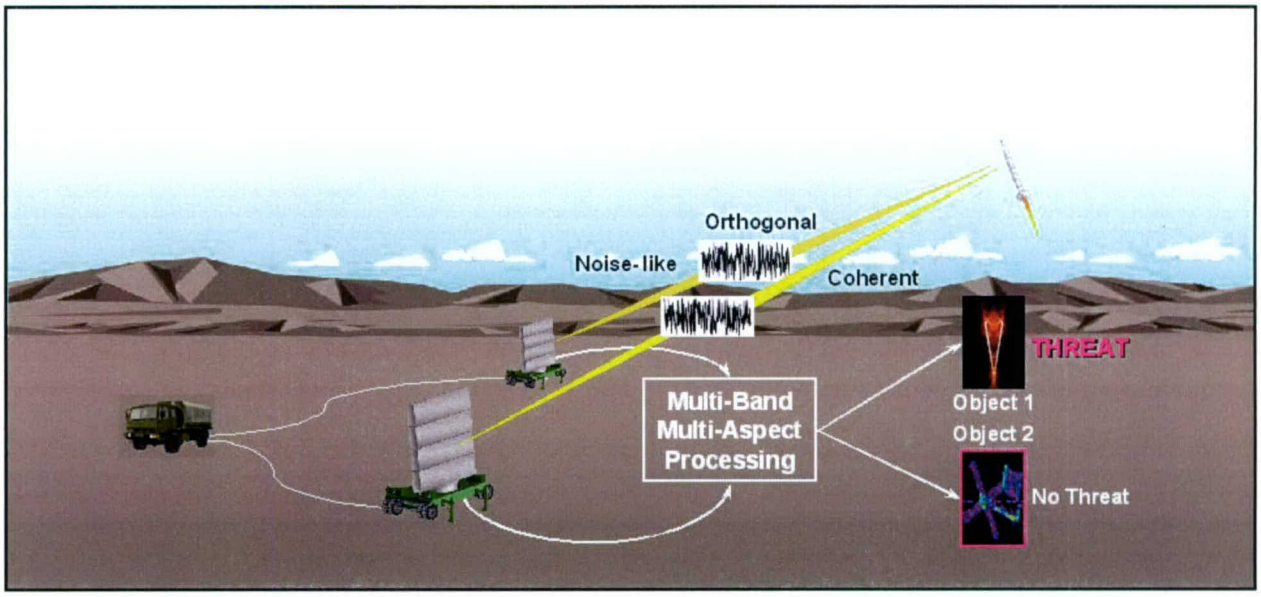

Figure 1. Conceptual architecture for coherently combining multiple radar apertures.

While joint operation of sensors can take on several levels of complexity, this report will focus on the development of aperture coherence algorithms for two (or more) nearly co-located radars having the same operating bandwidth and center frequency. We will show that by carefully controlling the transmit times and phases of the pulses from each radar aperture, the transmitted signals can be made to add together in a coherent and constructive way. This constructive interference will double the effective RF electric field impinging upon the target and provide an eight-fold increase in the power-aperture-gain product of two cooperative radars relative to one.

Cohering distributed wideband radar systems poses many new signal processing challenges. Our approach to achieving this level of multi-aperture coherence relies upon periodically separating the monostatic and bistatic return signals at each sensor so that fine timing/range and phase adjustments can be made to subsequent transmitted pulses. This separation assures that the coherence algorithms will work in non-reciprocal propagation environments. When two radars have achieved a true state of coherence on transmit, their waveforms will arrive at the target at the same time and in-phase. Consequently, the monostatic and bistatic received signals will also be coherently combined at each sensor. For reciprocal propagation environments, a generalized form of the conjugate beamformer (that includes time delays) may be used to maintain coherence.

To separate the monostatic and bistatic return signals, for the purpose of maintaining and updating the transmitter coherence parameters (fine timing/range and phase information), coded orthogonal waveforms can be used. The basic idea is to use a different orthogonal waveform at each transmitter and to separate the monostatic and bistatic returns at each receiver by matched filtering with the appropriate

replica waveform. This approach, however, generally requires the use of large time-bandwidth product waveforms in order to gain an acceptable level of isolation between the various radar return signals. In general, the height of the cross-correlation sidelobes for orthogonal waveforms is proportional to the waveforms time-bandwidth product. In cases where large time-bandwidth product waveforms can not be implemented, one may separate the multi-radar return signals using time-division-multiplexing (TDM) techniques. Specifically, a predetermined time delay can be added between the transmitted radar waveforms and the return signals analyzed to measure any time or phase deviations from this known condition. By analyzing the range and phase relationships of the monostatic and bistatic return signals, two otherwise independent radars can be made to operate in a coherent and cooperative way.

The MDA is currently sponsoring NGR under the Radar Systems Technology program. As part of the NGR design, laboratory and field experiments are being conducted to mitigate risks in the NGR system concept. Recently, in laboratory experiments we demonstrated the ability to cohere radar signals on receive with multiple antennas using an L-band radar test bed. We are also building and testing an X-band laboratory test bed that will demonstrate coherence on transmit and receive in real time (indoor static range tests in April 2004 have been very successful in demonstrating these concepts using real NexGen hardware. The results of these tests will be contained in a separate report). NGR field experiments will be conducted following the experiments with the X-band laboratory test bed. At this time the NGR field experiments are proposed for the final quarter of FY05.

Candidate test sites, and the site radars, were evaluated based on cost, availability, sensitivity, mobility, bandwidth, and ease of modification [5]. We concluded that the two AN/MPS-36 general purpose instrumentation tracking radars located on Kwajalein are the best choice for NGR field testing (see Figure 2). The Army has contracted with Lockheed Martin and Lincoln Laboratory to upgrade these radars with a Radar Open System Architecture (ROSA). This upgrade will provide the MPS-36s with flexible and maintainable COTS hardware and is scheduled to be completed in October of 2004.

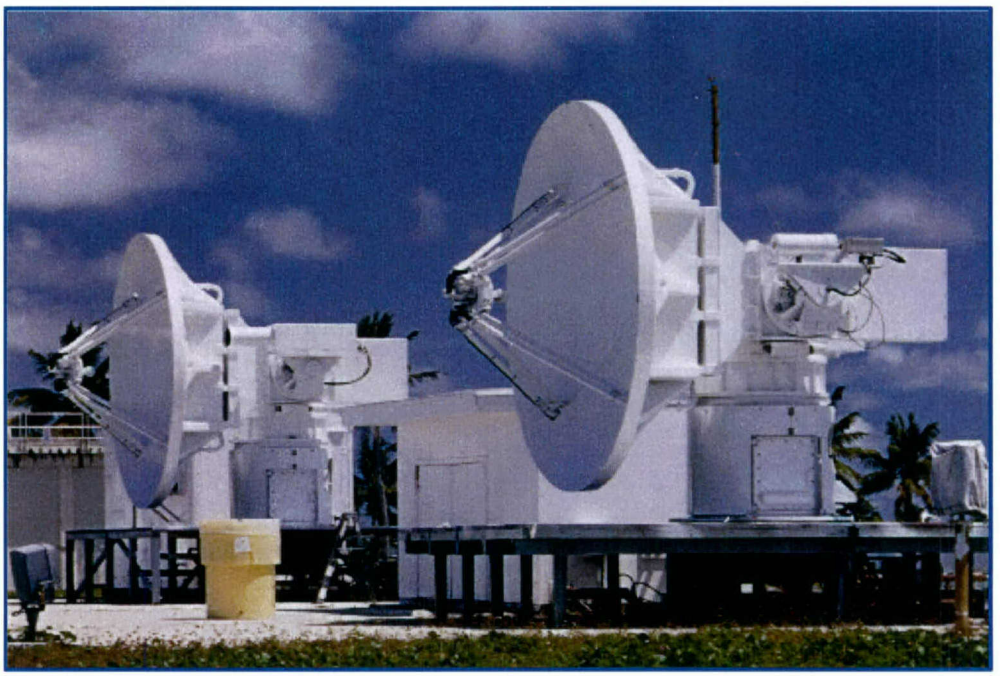

Figure 2. MPS-36 radars on Kwajalein.

1.1 EARLY WORK IN THE AREA OF DISTRIBUTED APERTURES

The use of distributed apertures to increase sensitivity and reduce the effect of atmospheric disturbances is not a new concept. Extensive work was carried out in this area in the late 1950s and early 1960s. Increased sensitivity was required at that time to support communications and telemetry with some of the first artificial and deep space satellites. The March, 1964 issue of the IEEE Transactions on Antennas and Propagation was a "special issue" dedicated to active and adaptive antenna techniques used to cohere multiple receiving elements and other related issues. The key technological enabler at the time was the phased-locked loop circuitry that permitted the development of *self-phasing* or *self-focusing* arrays of distributed apertures. Once a signal has been received at the array, some form of conjugate beamforming is employed to re-radiate or transmit back in the direction of the source or target. This type of antenna that transmits back in the direction of the received signal is called a retro-directive antenna.

The early papers in this 1964 special issue [6-8] recognized many of the benefits of distributed apertures that we anticipate today [9]. Some of these include:

1. Reduced cost. The cost per square meter of aperture is much less for distributed apertures versus a single large aperture.

2. Manufacturing tolerances are not as stringent for smaller apertures verses larger ones.

3. Antenna pointing or directing requirements are less stringent. Since the distributed aperture array is comprised of relatively smaller antennas with broader beamwidths, they do not require the tracking or directing accuracy of a single antenna with the equivalent aperture.

4. The self-phasing or self-focusing array does not require the propagation medium to be homogeneous thus allowing for atmospheric inhomogeneities. (However, the 1964 papers do not acknowledge that atmospheric inhomogeneities may be nonreciprocal.)

5. Differential Doppler shift from the target to individual antennas can be compensated for.

6. A conjugate beamforming system is indifferent to which particular grating lobe is chosen. Maximum gain is achieved and the system will correct to the main lobe of the combined antenna array.

7. A distributed aperture system is mechanically and electrically simpler than the equivalent single large aperture.

8. A distributed aperture system offers increased acquisition range for signal sources which are not known accurately in position.

Skolnik and King's paper [6] contains the first reference to the basic concept: "To the best of the author's knowledge, the concept of the self-focusing antenna was first proposed in the summer of 1958 by W.E. Morrow of MIT Lincoln Lab., Lexington Mass."

1.1.1 Self-phasing Antenna using Conjugate Beamforming

A self-phasing antenna senses the phase information incident across the aperture and uses this information in the proper manner to transmit a coherent signal back to the signal source or target. The shape of incident wave front need not be a plane wave. It could be spherical if the target is close to the apertures or it might be irregular due to atmospheric inhomogeneities. The basic self-phasing antenna that employs conjugate beamforming is shown in Figure 3.

The basic principal of self-phasing array using conjugate beamforming can be explained by examining one of the sub-apertures in Figure 3. We are considering the phase-only (narrowband) case in this argument, for wideband, the conjugate beamformer is generalized to include time delays as well as phase shifts. Starting at the target, let the signal reflected by the target be written as

$$\text{reflected signal} = A\cos(\omega t + \phi)$$

where A is the amplitude, ω is the frequency and ϕ is the initial arbitrary phase shift. The signal that arrives at the i^{th} aperture will be delayed by $T_i=R_i/c$ where R_i is the range and c is the velocity of propagation along the path. The received signal at the i^{th} aperture is written as

$$\begin{aligned}\text{received signal} &= A_i \cos(\omega(t - T_i) + \phi) \\ &= A_i \cos(\omega t - \omega T_i + \phi)\end{aligned}$$

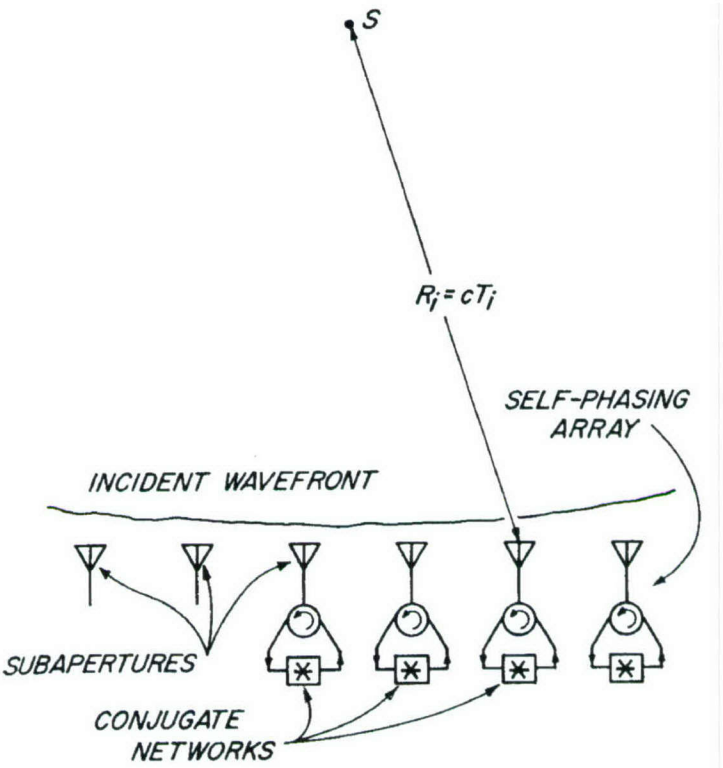

Figure 3. Self-Phasing antenna [6]. Irregular wave front incident on the sub-apertures of a self-phasing array antenna. T_i is the transit time from the source S to the i^{th} sub-aperture and c is the velocity of propagation.

where A_i is the amplitude at the i^{th} aperture. For transmit, the received signal phase in conjugated (i.e., the sign of the phase is reversed). Thus, the signal transmitted back to the target will be of the form

$$\text{signal radiated} = \cos(\omega t + \omega T_i - \phi)$$

where we have dropped the amplitude dependence A_i.

The signal transmitted by the i^{th} aperture will arrive back at the target with a propagation delay of T_i so that the signal returned to the target is of the form

$$\begin{aligned}\text{signal arriving at target} &= \cos(\omega(t - T_i) + \omega T_i - \phi) \\ &= \cos(\omega t - \phi).\end{aligned}$$

The argument of this signal is the same as the signal we started with except that the sign of ϕ, the initial arbitrary phase shift, has been reversed. Hence the signal radiated by the self-phasing antenna is independent of the transit time T_i. Thus the signals from all the apertures will have the same phase and combine coherently at the target no matter what the transit times from the individual apertures may be. (The fact the sign of the initial phase term has been reversed has no effect on coherence because it is the same for each subaperture and does not effect signal coherence.) To coherently combine the signals received at the N apertures, the phase at each aperture is shifted by the conjugate amount (i.e., set to zero) and the signals are combined as

$$\text{total received signal} = \sum_{i=1}^{N} A_i \cos(\omega t).$$

1.1.2 The Van Atta Array

The Van Atta array [10] is a special form of self-phasing conjugate-beamforming antenna that can be comprised completely of passive elements. It performs the conjugate operation by simple interconnections of the antenna elements. It can operate as a passive retro-directive antenna as shown in Figure 4 or can be made active by adding amplifiers in the transmit paths. The one-dimensional geometry shown can be directly scaled to two-dimensions. Unlike the general self-phasing array described above, the Van Atta array relies on a planer arrangement of elements and assumes that incident wave fronts are plane waves.

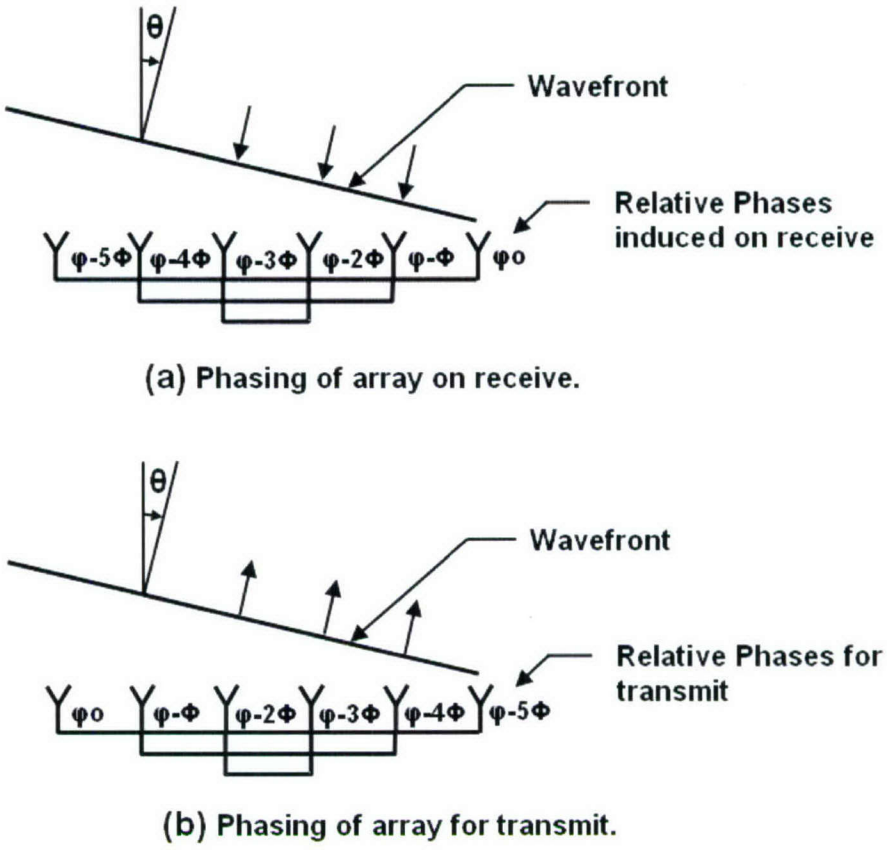

Figure 4. Van Atta Array achieves self-phasing through passive inter-element connections.

1.1.3 Early system using a four-element array of 30-foot dishes

We end the historic discussion with a brief description of a distributed aperture system that was developed in 1963. This system was developed as a research tool to demonstrate the principle of adaptively phasing the signals from independent array elements to achieve the same performance as a single equivalent aperture [8]. It was initially used in communication experiments involving the Echo I and Echo II passive satellites. A photograph of the antenna array is given in Figure 5. The receivers used phased locked loops with a common reference source to cohere the signals on receive. A single transmit antenna was used and they were successful in demonstrating the expected coherent gain of N during testing.

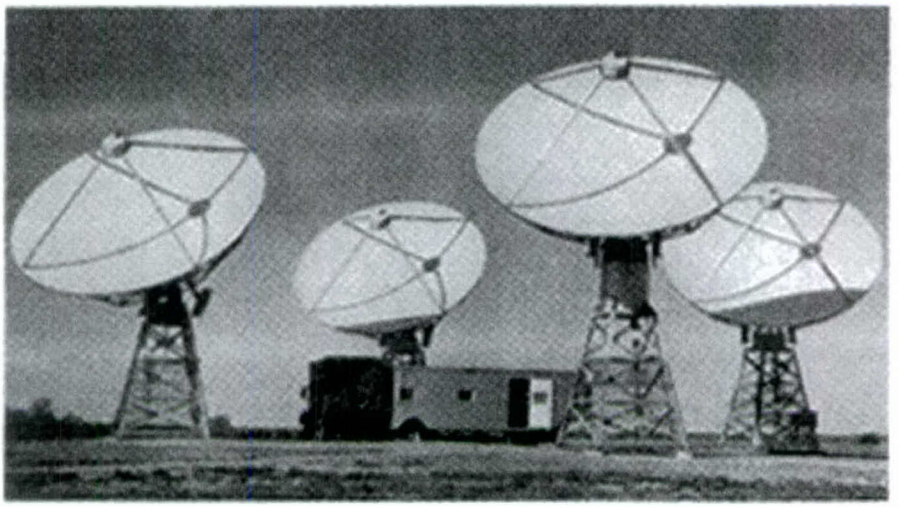

Figure 5. Four element array of 30-foot independently steerable parabolic antennas.

1.1.4 Why past work falls short

The historic work provides a good background for the current challenges but did not go far enough to meet our current needs. For example, the past systems were primarily narrowband communications systems, not wideband radar systems. Wideband systems require precise time alignment as well as phase alignment to achieve the desired coherent gain. Our use of orthogonal waveforms increases the array gain to N^2 instead of N for the single transmitter case above. Furthermore, when full coherence on transmit is achieved, the gain is N^3.

The past papers state that the self-phasing antenna is robust in the present of atmospheric inhomogeneities. However, this is only true when the atmosphere is reciprocal and this is not expected to be true for many geometries. We may have to wait until we collect data to determine the extent of the atmospheric inhomogeneities and the level of reciprocity. And finally, the venerability of a distributed aperture system to electronic counter measures (ECM) and the appropriate electronic counter-counter measures (ECCM) must be considered.

Developing the signal processing engine to cohere multiple wideband radar apertures on a target is a complex technical challenge and our approach to this problem is still evolving. This report should be regarded as a "work in progress" document that takes a first step forward towards addressing some of the issues involved.

The report is organized as follows. In Section 2, we discuss signal processing architectures for estimating the multi-radar coherence parameters from the monostatic and bistatic return signals. In Section 3, we present a number of coherence parameter extraction algorithms, evaluate their performance against theoretical bounds, and compare their computational complexity. Section 4 summarizes our conclusions and recommendations for performing real-time aperture coherence experiments in the field.

2. WIDEBAND APERTURE COHERENCE ARCHITECTURES

The basic idea behind multi-radar aperture coherence is straightforward - transmit at the right times and with the proper phases so that the radar energy coherently combines at the target. At first look, this would seem to imply that the position of the target and radars are precisely known. And, it would also seem to require very fine control of transmit times and phases in order to accomplish this task. Another practical issue has to do with target motion; by the time we estimate the proper coherence parameters to use, the target would have moved, so are the transmit times and phases now wrong? Finding simple ways to overcome these potential coherence problems in real radar systems is what this section of the report will begin to address.

We begin by assuming that the NGR receives a target cue from forward-based sensors (or some other means). The cue is typically in the form of a state vector and other relevant information concerning the type of target(s) to be acquired. The NGR then begins its search and acquisition phase as a group of radars using orthogonal waveforms. There are four standard phases of radar operation: (i) search; (ii) acquisition; (iii) track; and (iv) cohered track. The search mode will be cued and searching will consist of a scan, with coherent and/or non-coherent integration in the vicinity of the target. Once a contact has been made, the NGR will dwell attempting to increase the SNR through longer integration times. During acquisition the NGR can use a combination of coherent and non-coherent integration to increase the SNR. After acquisition, the NGR will shift to tracking mode and cohere on transmit and receive to track the target at maximum SNR. This track will generally be formed at narrowband. The narrowband state vector can then be used to align the target returns within each radars wideband range window; in principle, the radar's bandwidth can be gradually stepped-up to provide a smooth transition from narrowband to wideband operation. The state vectors can also be used as a stable phase reference for subsequent wideband range-Doppler imaging or coherent pulse integration applications. Wideband operation with full coherence provides the highest resolution and SNR to support precision track and target discrimination. The target can be discriminated using a variety of target metrics (e.g. length, size and shape, PP/OP ratio, etc.). The four NGR processing phases are depicted in Figure 6.

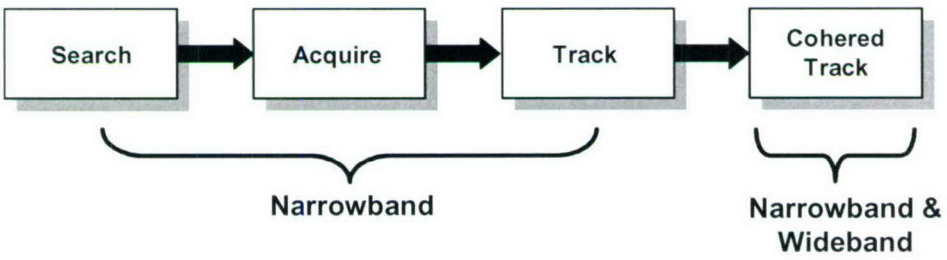

Figure 6. Next Generation Radar processing phases.

To describe this process in more detail, consider Figure 7 which shows a flow diagram of how a typical NGR might operate during the search through tracking phases. We have not necessarily assumed that the individual base units within the NGR cluster are able to acquire on their own. Consequently, a combination of coherent and/or non-coherent integration across pulses and platforms may need to be employed. For most scenarios; however, the base unit will be able to acquire and track the targets on their own. The extra SNR obtained by combining multiple base units supports precision track and discrimination.

Orthogonal waveforms will be used during search and acquisition to provide a broad beam pattern. Each base unit initially operates independently and uses a combination of coherent and non-coherent integration to boost it's SNR in an attempt to acquire the target. Once a target is acquired, the central computer is initialized and begins to accept tracking information and raw I/Q data from the base units. Non-coherent integration would typically be used in the central computer to improve the tracking performance of the cluster relative to any one base unit. The central computer would gradually take over the tracking function by sending state vector information back to each base unit. The base units would continue to send raw I/Q data to the central computer. The central computer will calculate cross-platform coherence parameters and attempt to cohere on receive at narrowband. This will, in principle, significantly improve the SNR and tracking quality of the NGR cluster.

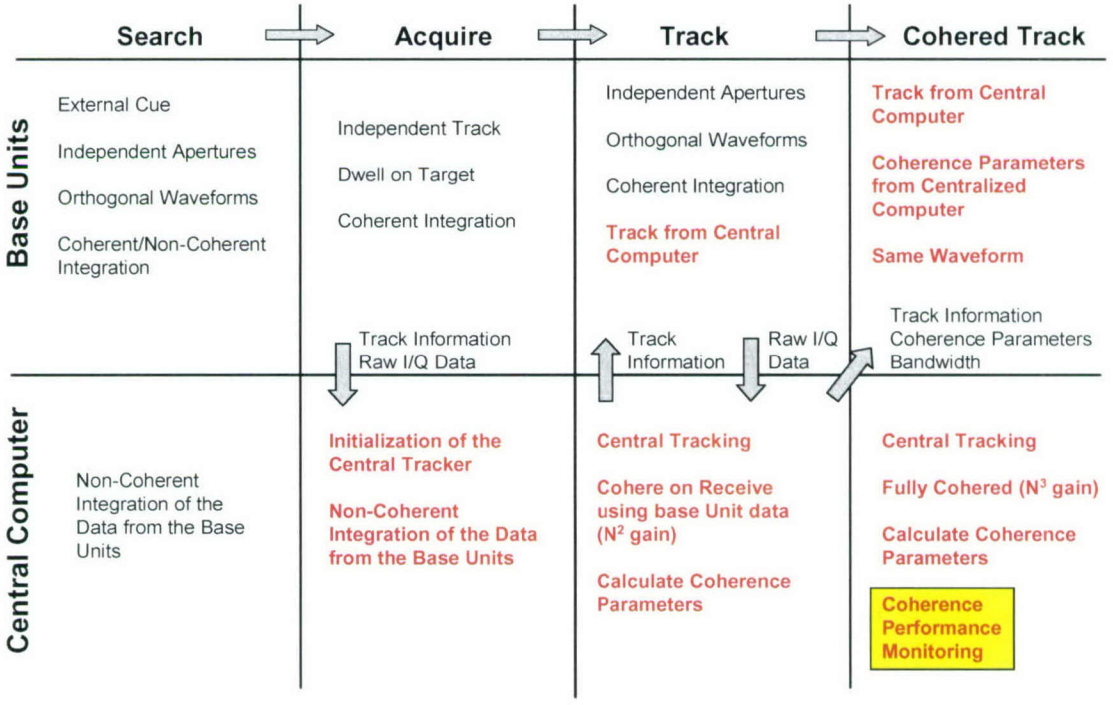

Figure 7. Next Generation Radar processing flow.

The NGR transitions to the cohered tracking mode when the central computer begins to send coherence parameter updates to the base units. The base units can be switched to using the same waveform; at this point, the central computer's coherence algorithms will cohere the base units on transmit and receive.

Coherence parameter tracking and updating is an important part of the NGR back-end data processing operation. (The radar front-end processing, including digital in-phase and quatrature (DIQ), pulse compression, beamforming, etc., is not discussed here.) To make things a bit more concrete, we will now consider in detail the case where the transmissions from two wideband radars are to be mutually cohered. Theoretically, the range difference between the radars and the target can be used to define initial timing and phase offsets in an attempt to provide a course level of coherency. Specifically, if the range from radar 1 to the target is denoted by R_1 and the range from radar 2 to the target is denoted by R_2, initial estimates of the difference in transmit times, Δt, and transmit phases, $\Delta\phi$, of radar 1 relative to radar 2 are given by equations 1 and 2, respectively.

$$\Delta t_0 = \frac{R_1 - R_2}{c} \tag{1}$$

$$\Delta \phi_0 = \frac{2\pi(R_1 - R_2)}{\lambda} \tag{2}$$

The constant c is the speed of propagation and λ is the center wavelength of each radar. Throughout the report, we will refer to Δt and $\Delta\phi$ collectively as coherence parameters. By using the initial coherence parameters stated above, we are attempting to make the two radar waveforms arrive at the target at the same time and be in-phase.

It is important to note that equations (1) and (2) are to be used for initial coherence parameter estimates only. The target tracker range estimates will not, in general, be accurate enough to provide truly coherent operation. However, by analyzing the relative range and phase relationships of the monostatic and bistatic return signals, appropriate coherence parameter adjustments can be made to the transmitted waveforms. If a radar's monostatic return comes back first, i.e. before the bistatic returns, it needs to slow down and retard it's transmit phase appropriately. The opposite is true if the bistatic returns are received first. This forms a closed-loop process which, in principle, will bring the radars closer to operating in a mutually coherent way. The key point here is that precise information regarding *the absolute position of the radars and target is not critical* for making appropriate adjustments to the multi-radar coherence parameters. However, a closed-loop real-time signal processing architecture is needed to make this work. Below, we discuss and illustrate two signal processing architectures for accomplishing this task.

In Figure 8, we show a target being illuminated by two wideband radars. After matched filtering, the monostatic and bistatic returns observed at the "master" radar are separated into channels using orthogonal waveform processing or the TDM technique discussed previously. The relative range and

phase relationships of these returns signals are then compared so that optimal adjustments can be made to the transmit time and phase of the "slave" radar pulses.

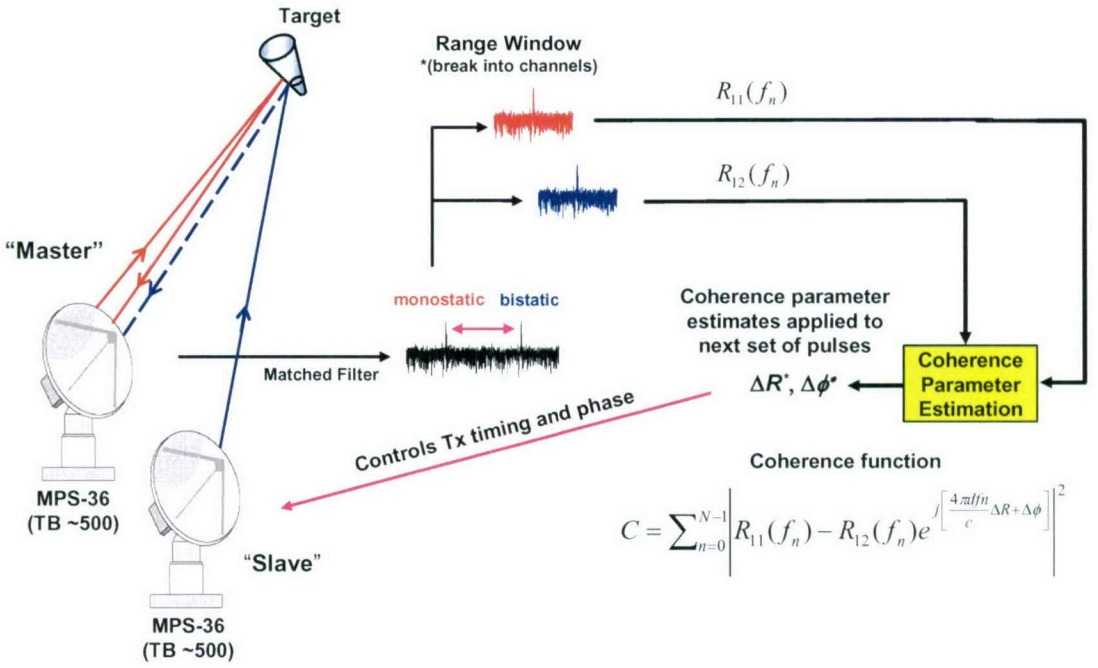

Figure 8. Master-slave radar architecture.

This signal processing architecture is relatively simple to implement due to the fact that all of the data processing occurs at the master sensor. The slave sensor(s) simply accepts coherence parameter updates from the master and thus the overall signal processing and communication requirements between sensors are minimized. When only a single slave sensor is used, the master sensor can adjust its own transmit delay and phase to match that of the slave to minimize communications even further. In either case, the slave sensor needs to communicate the coherent target I/Q data so that it can be combined at the master sensor to achieve the N^3 SNR gain. There are many ways to correlate the radar return signals for the purpose of estimating the coherence update parameters. This will be discussed in Section 3 of the report. Below, we discuss and illustrate an alternative and more robust signal processing architecture.

While the master-slave configuration looks interesting, it is also clearly suboptimal – the return signals at the slave radar have been ignored in the computation of the coherence parameters. To make

better use of all of the available radar measurements, we need to process the monostatic and bistatic return signals from both radars at the same time. A signal processing architecture for accomplishing this kind of data fusion is shown in Figure 9. In this figure, the relative range and phase relationships of the monostatic and bistatic returns are compared at **both** sensors. This "cooperative" radar architecture provides an improvement in processing gain for the coherence parameter estimates relative to the master-slave arrangement in Figure 8. The cooperative architecture processes all four return signals whereas only two return signals are processed in the master-slave architecture. The cooperative processing approach, however, requires roughly twice as much computer resources to implement and the communication link between sensors is also somewhat more sophisticated.

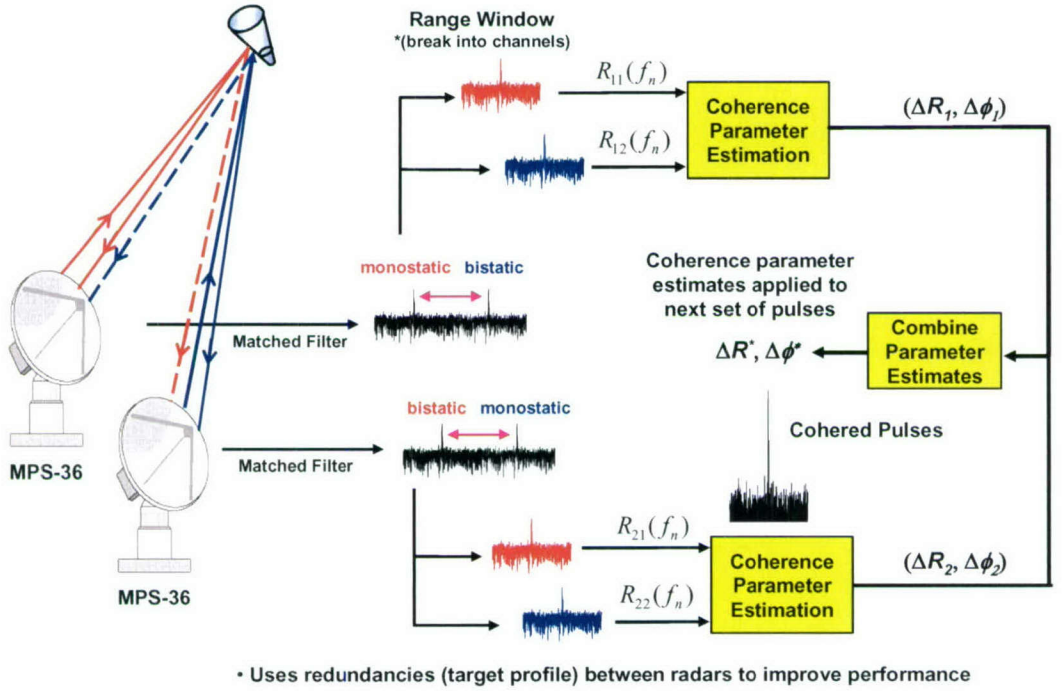

Figure 9. Cooperative radar architecture.

Coherence performance monitoring also needs to be performed in real-time to verify the accuracy of the parameter updates. When using a single waveform, the monostatic and bistatic returns will be combined at each sensor. Coherence error estimates can be obtained by cross-correlating the returns

across platforms. The peak of the cross-correlation function defines the location and phase errors between the combined returns. The central computer can then correct for these coherence errors appropriately. A potential difficulty with this approach is that it is not possible to separate transmit from receive paths caused by drift in the sensor transmit and/or receive chains, or due to a non-reciprocal troposphere. In cases where the coherence errors appear to be large, however, the central computer can switch the base units back to using orthogonal waveforms so that the base units can be re-cohered as indicated in Figure 10.

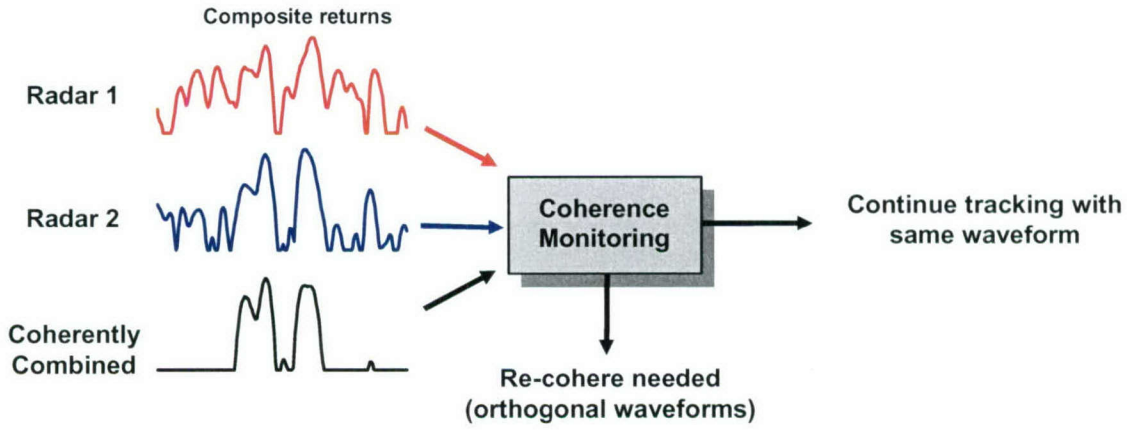

Figure 10. Coherence monitoring function.

Robust real-time coherence monitoring algorithms are currently under development. The cross-platform correlation technique is one possible approach to monitor coherence. We are also investigating more sophisticated techniques involving coherence functions, measures of entropy (signal self-similarity), and auto-correlation techniques to measure "blur" in the composite radar returns.

Below, we consider various methods for extracting the coherence parameters from the monostatic and bistatic return signals when orthogonal waveforms are being employed.

3. COHERENCE PARAMETER ESTIMATION ALGORITHMS

As discussed in Section 2, to cohere multiple radar apertures on transmit and receive we have assumed that the target is in track and a smooth state vector has been formed. The range from the radars to the target can be used to provide initial estimates of the coherence parameters. Fine timing and phase adjustments to the transmitted waveforms can then be made using the master-slave or cooperative radar architectures also discussed in Section 2. This forms a robust closed-loop process that uses the received data to "lock" the radars together in a mutually coherent way.

To make this process work in real-time, range-marking algorithms are needed to detect and measure the targets position (fine range and phase) within each radars wideband range window. There are several potential ways to accomplish this task. The approaches vary widely – they can be as simple as "peak picking" or as sophisticated as using multi-pulse all-pole signal models to super-resolve and align the monostatic and bistatic target images. Whichever method is employed, however, the main goal is to use the target information available from the received data to make fine timing and phase adjustments to the transmitted waveforms so that the monostatic and bistatic returns are coherently combined at the receiver.

The coherence parameter extraction algorithms that we will consider in detail in this report are listed below.

1. Peak picking
2. 1D cross-correlation processing
3. 1D all-pole modeling
4. Multi-pulse integration with cross-correlation
5. Multi-pulse integration with all-pole modeling
6. 2D all-pole modeling

Below, each of these algorithms is briefly discussed. In Section 3.2, we compare the experimental performance of these algorithms to the Cramer-Rao lower bound. Section 3.3 demonstrates cohere on receive performance using complex target data collected on a static test range. In Section 3.4, we consider the real-time computing requirements of each algorithm.

3.1 COHERENCE PARAMETER EXTRACTION

3.1.1 Peak Picking

As mentioned above, "peak picking" is the simplest approach for estimating the multi-radar coherence parameters. This technique involves locating the target's peak signal power in both the monostatic and bistatic compressed pulses. The range separation, $\Delta R = R_{mono} - R_{bistatic}$, between the monostatic and bistatic returns defines the timing offset correction via equation (3).

$$\Delta t = \frac{R_{mono} - R_{bistatic}}{c} = \frac{\Delta R}{c} \tag{3}$$

The phase correction, $\Delta\phi$, is derived by measuring the target's phase response at the peak of the monostatic and bistatic returns. Note that the phase correction is also a function of the estimated range separation, ΔR, as indicated in equation (4).

$$\Delta\phi = \frac{-2\pi\Delta R}{\lambda} + \left(\phi_{mono} - \phi_{bistatic}\right) \tag{4}$$

Because this method relies upon the relative range and phase of a single target scatterer, it is not expected to perform as well on complex targets or at low signal-to-noise ratios (SNRs) as some of the more sophisticated methods discussed below.

3.1.2 1D cross-correlation processing

In this method, the wideband monostatic and bistatic compressed pulses are cross-correlated. The peak of the cross-correlation function defines the range separation, ΔR, between the monostatic and bistatic return signals and can be used in (3) to provide the closed-loop timing offset correction. The phase at the peak of the cross correlation function defines the phase difference, $\phi_{mono} - \phi_{bistatic}$, between the monostatic and bistatic returns and can be used to provide the closed-loop phase offset correction in equation (4).

Because correlation processing uses the full extended range return of the target to update the coherence parameters, it is expected to perform better on complex targets and/or at lower SNRs than peak picking. To improve the resolution and/or to further reduce the amount of noise present in the received data, modern spectral estimation techniques may be used. This approach to coherence parameter estimation is discussed below.

3.1.3 1D all-pole modeling

In 1D all-pole modeling, the original "noisy" received pulses are replaced by a data-derived parametric signal model of the target. The use of all-pole signal models to represent radar backscatter from metallic targets is well-known in the signal processing literature (see [1-4,11-12] for examples). The monostatic and bistatic compressed pulses are range windowed and inverse Fourier transformed back into their respective in-phase (I) and quadrature-phase (Q) signal components. This process decompresses the signal returns and this data is then subjected to the all-pole modeling procedure.

The details behind all-pole signal modeling can be found in [1,2]. The basic idea is to optimally fit a signal model of the form

$$S(f_n) = \sum_{i=1}^{P} a_i p_i^{\,n} \tag{5}$$

to the uncompressed (frequency domain) data samples. In (5), the constant P corresponds to the estimated number of discrete scattering centers on the target, the a_i are the complex amplitudes of the scattering centers (RCS and phase), and the p_i are the corresponding poles (relative range locations) associated with each scattering center. It is important to note that all of these model parameters are determined strictly from the target response data, i.e. no assumptions are required regarding the number of scattering centers, their locations, or amplitudes and phases.

Once the monostatic and bistatic signal models have been estimated, "clean" compressed pulses are formed by applying standard Fourier processing techniques to the corresponding signal models. The correlation processing approach can then be applied to these compressed pulses to estimate the range separation and phase difference between the monostatic and bistatic return signals. The primary advantage of signal modeling is that it removes some of noise from the target signal prior to correlation processing. Thus, it is expected to perform better with complex targets and/or at lower SNRs than standard correlation processing.

3.1.4 Multi-pulse integration with correlation processing

A common method for "building up" the SNR on the target is to pre-sum a number of pulses. This requires that the target returns are aligned in range and phase prior to integration. Range alignment typically needs to be accurate to some small percentage of a range resolution cell whereas phase alignment requires that the phase of the returns be consistent with their relative range to within a small percentage of the radar's center wavelength. This generally requires that a smooth and stable wideband target track be established before the pre-summing can occur. Pulses can be summed either coherently or non-coherently depending on the accuracy of the alignment and complexity of the target. Coherent integration typically improves SNR by a factor equal to the number of pulses integrated, assuming that the scattering centers are not fluctuating over the coherent integration time interval.

Once the pulses have been integrated, the previously discussed methods can be applied to estimate the range and phase offset between the bistatic and monostatic returns. In particular, correlation processing can be used to provide robust estimates of the multi-radar coherency parameters.

3.1.5 Multi-pulse integration with all-pole modeling

This approach is similar to the method discussed above except that an all-pole signal is used to improve the range resolution of the pre-sum pulses prior to correlation processing. As noted earlier, the use of all-pole signal models tend to improve the performance of correlation processing when the targets are complex and/or the SNR is poor.

3.1.6 2D all-pole modeling

Multi-dimensional all-pole modeling is considered an advanced concept [4,12] – a brief summary of the approach is provided below. We mention it here because of the far term potential that multi-dimensional signal modeling provides for helping to mitigate severe clutter. These methods are also routinely used at Lincoln Laboratory to coherently combine radar measurements taken from sensors operating at different PRFs and on different frequency bands. This allows the generation of super-resolved ultra-wideband target images from which detailed target features can be extracted and advanced discrimination functions performed.

A summary of the processing flow for 2D all-pole modeling is illustrated in Figure 11. In conventional image processing, a block of radar pulses is collected over a given frequency bandwidth and time period to obtain resolution in range and Doppler. This same block of pulses may also be used to form a two-dimensional (frequency-time) all-pole signal model of the target from which a super-resolved target image can then be obtained. The resulting all-pole model images typically show considerably more target detail than conventional FFT-based images. The improvements in resolution and processing gain makes 2D all-pole modeling a powerful method for robustly estimating the target coherence parameters (range and phase offsets) in very noisy environments. The images also provide target Doppler correction information which is important for cohering multiple radar apertures that operate on different frequency bands, are spatially separated, or use broadband noise-like waveforms. Details of the 2D signal modeling algorithm are reported in [4,12] along with several applications to field data.

An added advantage of representing a block of wideband radar return signals by an "equivalent" frequency-time signal processing model is that the signal model fully exploits the correlation properties of the target relative to unwanted noise. Moreover, the signal model poles correspond to super-resolved scattering center locations in an image of the target. By tracking the motion of these signal poles in the range-Doppler image plane as time-overlapped data blocks are sequentially processed, we can often detect and image targets in highly cluttered environments where conventional linear imaging methods typically fail.

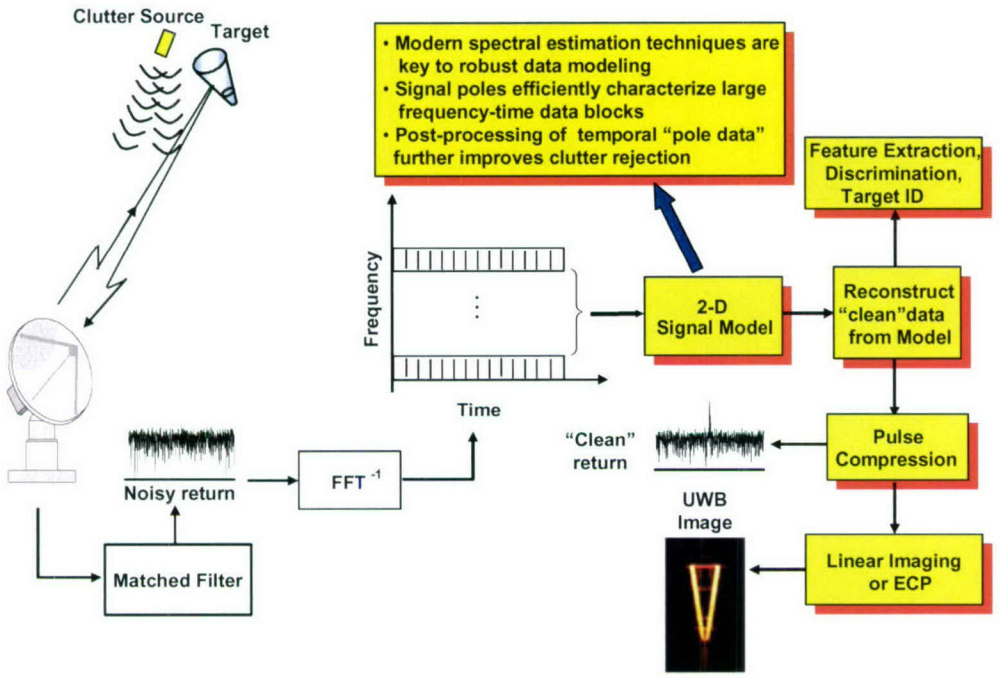

Figure 11. Two-dimensional block processing methodology.

This approach to advanced clutter rejection processing is further described in Figure 12. A sliding window of frequency-time data blocks are sequentially processed in time using a two-dimensional all-pole signal model. The signal model parameters represent the original data blocks in a robust and efficient way. The signal model poles are tracked from frame to frame until the target signal can be reliably separated from the clutter returns. The basic assumption here is that the clutter will eventually decorrelate, in time and/or frequency, relative to the scattering from a rigid metallic target. This allows the target to be detected and imaged at much lower signal-to-clutter ratios than possible with conventional linear image-based techniques.

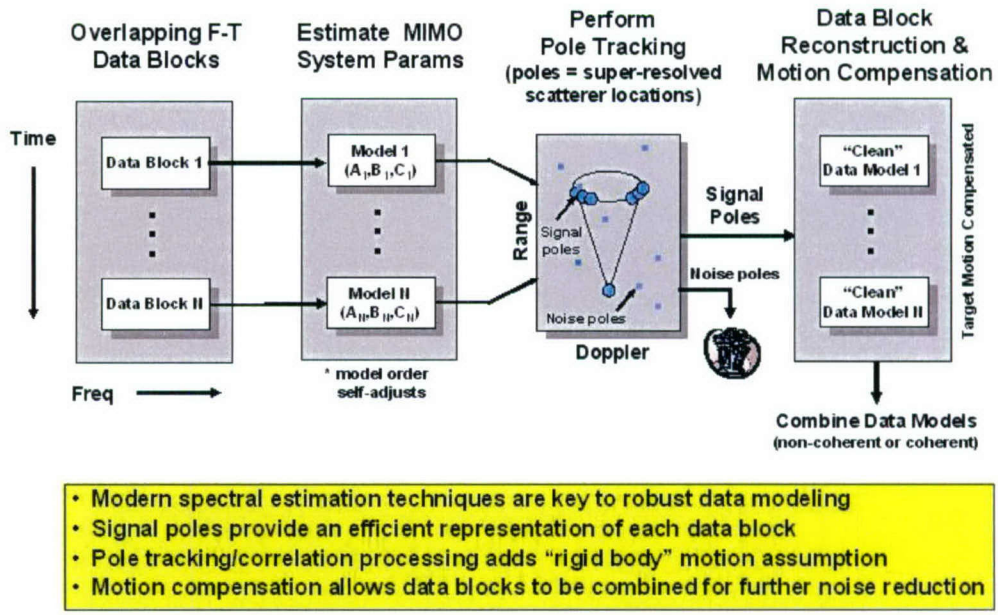

Figure 12. Advanced clutter rejection processing.

While this algorithm has been successfully demonstrated using a wide variety of simulated and field data collected on targets that are deeply embedded within clutter, the approach is computationally intensive. Much work remains to make 2D all-pole modeling realizable in real-time hardware for BMD applications. Computational complexity comparisons for the various coherence options discussed above are provided in Section 3.3 of this report. Below, we evaluate and compare their performance against theoretical bounds.

3.2 POINT-SCATTERER PERFORMANCE BOUNDS

It can be shown [13] that a radars range and phase estimation performance depends on the signal bandwidth and signal-to-noise ratio. Assuming that the radar illuminates a simple point target and that the noise is white and Gaussian, expressions for the range and phase estimation errors are given, respectively, by

$$\sigma_{\Delta R} = \frac{c/2B}{\sqrt{2 \cdot SNR}}$$

$$\sigma_{\Delta \phi} = \frac{1}{\sqrt{2 \cdot SNR}}$$

where B is the radar's bandwidth. The equations above will be used as a baseline for comparing the performance of our various coherence parameter estimation algorithms.

The master-slave architecture estimates the target's multi-static range and phase offsets using a single radars monostatic and bistatic received signals. The cooperative architecture, on the other hand, uses all N^2 return signals. Consequently, the cooperative architecture should produce coherence parameter estimates with smaller errors (for N=2, the errors should be smaller by about 3 dB).

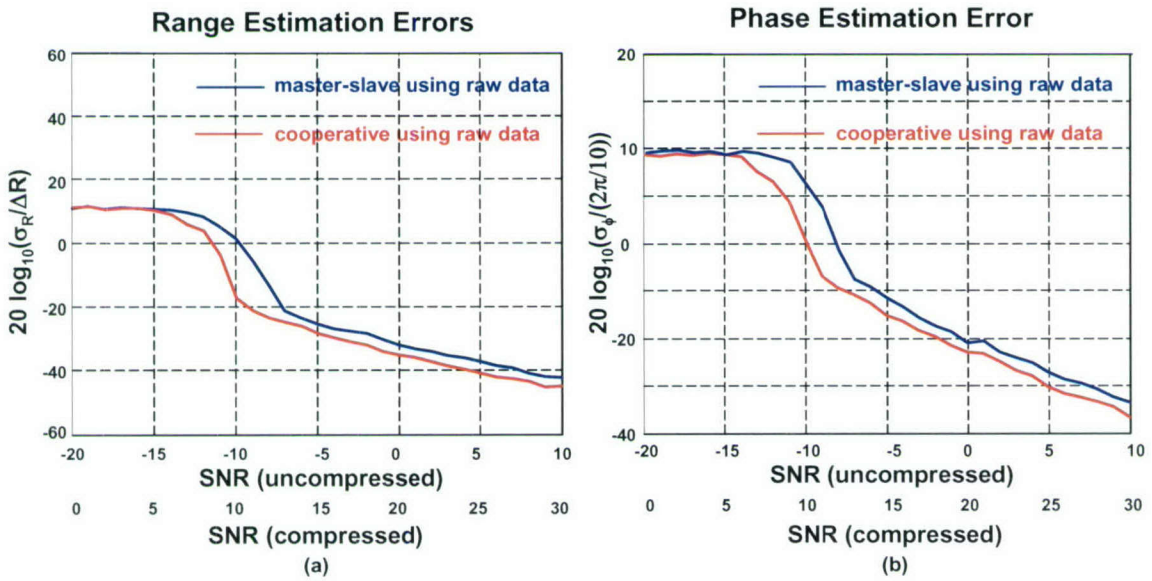

Figure 13. Single-pulse algorithm performance using correlation processing: (a) Range estimation error for master-slave and cooperative radar architectures; and (b) Phase estimation error for master-slave and cooperative radar architectures.

To show this comparison, consider Figures 13(a) and (b) which show the range and phase estimation errors for a single point-scatterer using a Monte Carlo simulation of the master-slave and cooperative radar coherence architectures discussed in Section 2. For clarity, only the performance of the raw data correlation method is shown here. Note that the cooperative radar architecture outperforms the master-slave architecture by about 3 dB, as expected. The breakpoints (where the curves begin to increase sharply as the SNR decreases) show that the master-slave estimation errors are small for single-pulse SNRs greater than about 13 dB. The cooperative radar architecture performs well down to SNRs of about

10 dB. Pulse integration methods may be used to improve the SNR prior to coherence parameter estimation as discussed in Section 2. By coherently integrating ten pulses, for example, the curves illustrated above will shift approximately 10 dB to the left, or by about 5 dB if non-coherent pulse integration is used.

It is also interesting to study the performance of the peak picking and pole-based parameter extraction algorithms. In Figures 14(a) and (b), we show the range and phase estimation performance of the cooperative processing architecture using three different feature extraction algorithms – peak picking, raw data correlation processing, and all-pole model correlation processing. Also shown is the corresponding Cramer-Rao lower bound. Because the target is assumed to be a single isolated point-scatterer, it is not surprising that the performance of these three algorithms is very similar. One important distinction, however, is that all-pole modeling has approximately a 5 dB lower SNR breakpoint than standard correlation processing. This is due primarily to the singular-value-decomposition (SVD) step in the all-pole modeling algorithm. The SVD tends to reject some of the noise components present in the signal. This improvement in performance comes at the expense of increased computational cost as will be discussed in Section 3.4.

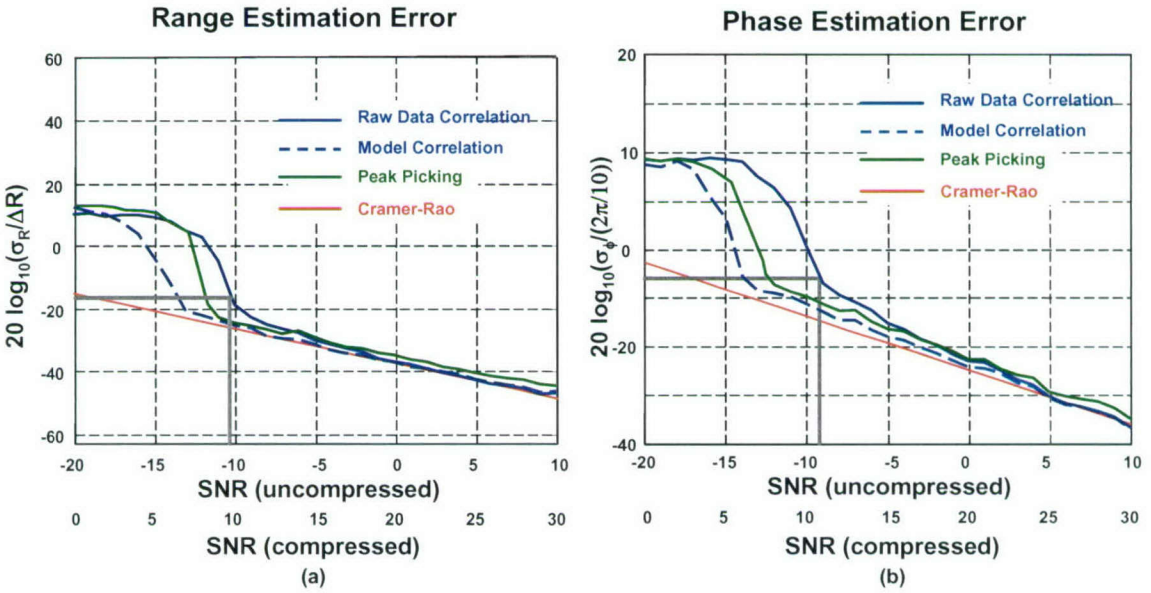

Figure 14. Single-pulse cooperative radar architecture algorithm performance using peak-picking (green curve), correlation processing (solid blue curve), and all-pole modeling (dashed blue curve): (a) Range estimation error; and (b) Phase estimation error.

It should be noted that these results are for a single point-scatterer and that true performance will depend on many factors, including target complexity. When the target consists of two or more competing scatterers, as shown in Figures 15(a) and (b), the peak picking method will, in general, fail due to difficulties in consistently aligning the bistatic and monostatic target returns. For complex targets, correlation processing is generally considered more robust because the entire target extent is used for range and phase estimation purposes. And if computational resources are sufficient, all-pole modeling techniques may be used to reduce unwanted noise and potentially further improve performance.

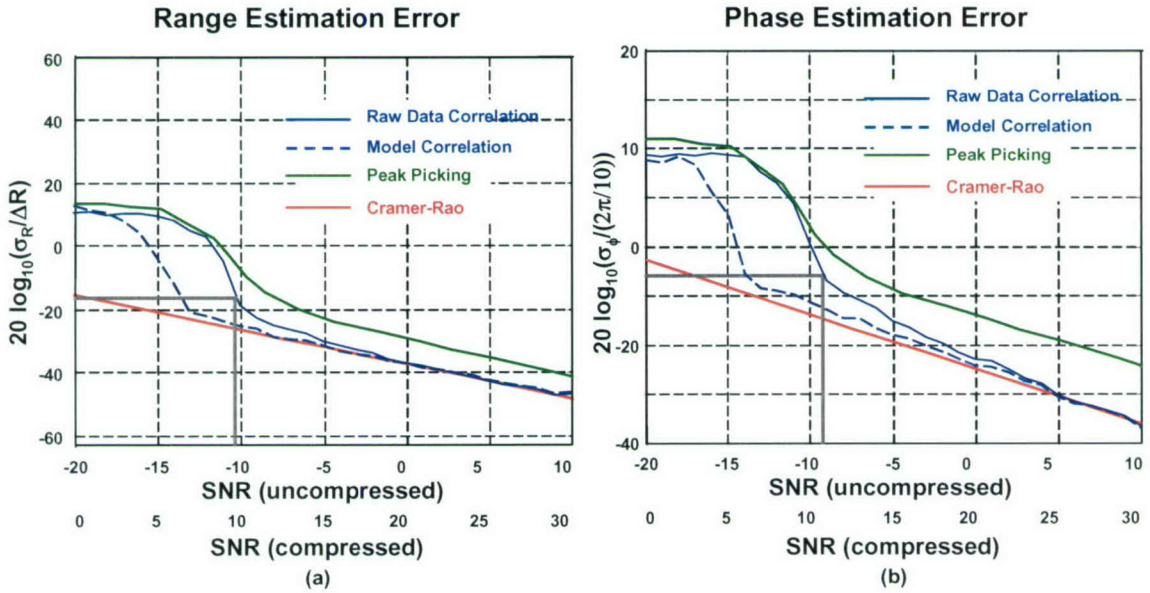

Figure 15. Two Scatterer, single-pulse cooperative radar architecture algorithm performance using peak-picking (green curve), correlation processing (solid blue curve), and all-pole modeling (dashed blue curve): (a) Range estimation error; and (b) Phase estimation error.

It is also interesting to study multi-radar coherence performance in terms of SNR gain-loss curves, as shown in Figure 16 [14]. Ideal coherence is achieved if it was possible to perfectly aligning and phase match all four target returns (two bistatic and two monostatic) at the receiver. In this case the coherence gain at the receiver would be about 6 dB, corresponding to a SNR gain-loss of 0 dB. When the data is noisy, range and phase estimation errors are inherent and, therefore, performance will be less than ideal. Note also that Figure 15 shows a breakpoint in the curves at around a 10 dB single-pulse SNR. At this level of SNR, the master-slave architecture (blue curve) provides only about 5 dB of coherence gain (1 dB

gain-loss), whereas the cooperative architecture (red curve) provides about 5.8 dB of coherence gain (0.2 dB gain-loss). At higher SNRs, the gain-losses converge to zero for the two estimators and at lower SNRs in the 5-10 dB range, the gain loss is about 1.5-2 dB.

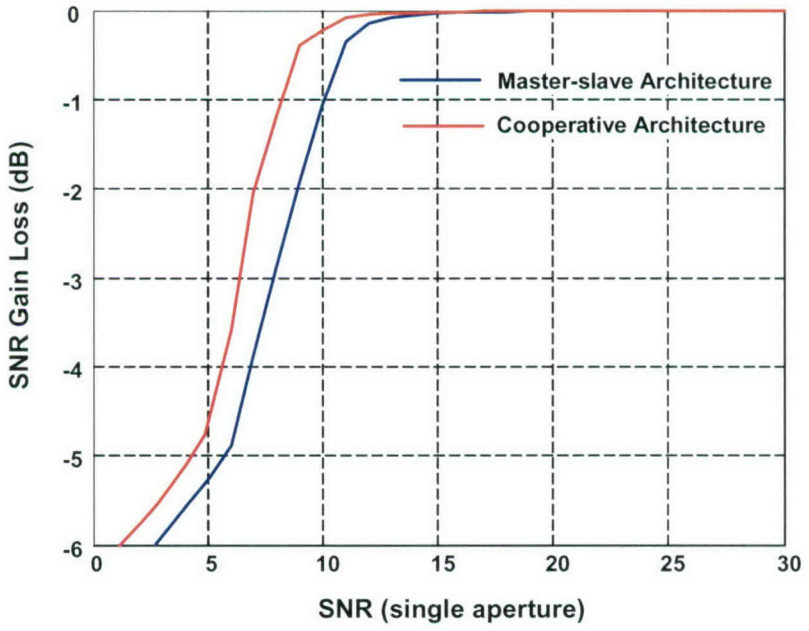

Figure 16. Radar "receive" coherence in terms of SNR gain-loss. The SNR gain loss is defined for a single point-scatterer using a standard sinc radar waveform.

3.3 STATIC RANGE MEASUREMENTS AND ANALYSIS

In this section, we use static range measurements on a scale reentry vehicle (RV) to check the performance of our coherence parameter estimation algorithms on a complex target. Radar measurements on the target shown in Figure 17 were collected over a 2-18 GHz frequency range. We will focus our experiments at X-band, from 9.5-10.5 GHz, as illustrated in the figure. Scattering from the nose-tip, base edge, and several grooves/ridges located along the body axis are readily apparent over this frequency range. Below, this data is used to simulate the monostatic and bistatic returns that two real X-band sensors might see.

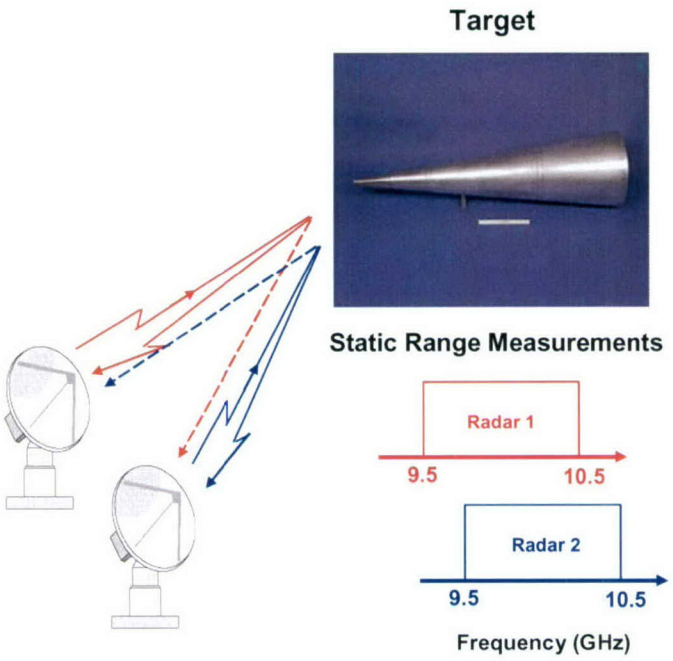

Figure 17. Complex target static range measurements to demonstrate coherence processing.

In Figure 18, multi-static RTI plots are shown. These plots were generated using data collected over a full range of aspect viewing angles of the target. Known range and phase biases were introduced into the static range measurements to simulate the effects of two X-band sensors transmitting and receiving at nearly the same time. The range bias, in this example, is a constant 3 meters for all of the radar aspects shown, while the phase bias is zero degrees. The single pulse SNR level is 5 dB. Notice that two radars, both transmitting and receiving, comprises four (N^2) independent looks at the target – each receives its own monostatic response plus the bistatic returns from the other radars. In this example, the monostatic and bistatic returns can be separated in range due to the relatively large range offset between the two simulated sensors. In general, orthogonal waveforms would be used to channelize the monostatic and bistatic target responses so that accurate estimates of the coherence parameter offsets can be made, even when the monostatic and bistatic returns overlap.

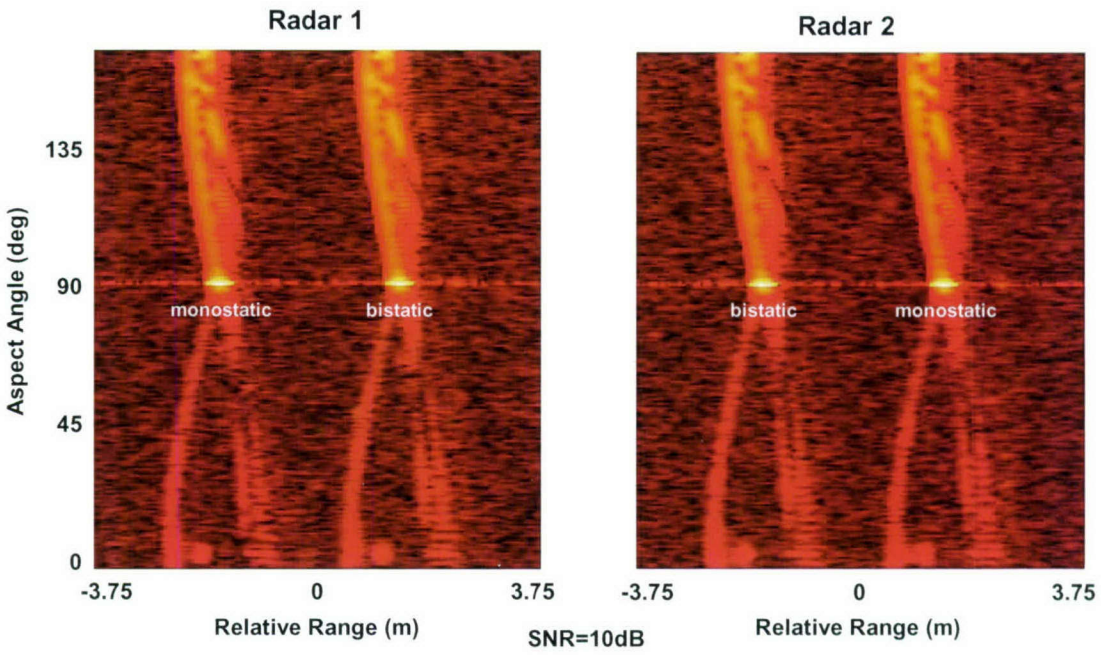

Figure 18. Complex target range-time-intensity plots. Two radars transmit and receive. Goal is to align and coherently combine the two monostatic and bistatic returns so as to simulate two radars operating in a mutually coherent way.

To cohere radars 1 and 2 on receive, the cooperative radar processing architecture can be used. Recall that this architecture estimates the range and phase offsets between the monostatic and bistatic return signals using all N^2 target returns. The master-slave architecture could also be used, but in this case, performance of the coherence parameter estimator would be degraded by about 3 dB (due to using the data from only one sensor) and the corresponding SNR gain-loss would increase by .5-2 dB depending upon SNR.

Figure 19 shows the result of applying the cooperative radar processing architecture to estimate and track the range and phase bias for cohere-on-receive processing. Single-pulse range marking was used to compare cross-correlation processing to the peak picking method. Note that the coherence parameter estimates resulting from cross-correlation processing are much more reliable than the peak picking results (red curves). Because the target exhibits multiple scattering centers with similar RCS levels, the peak picking method can not reliably align the target returns on a pulse by pulse basis. The cross-correlation technique also exhibits considerable variation at some aspect angles, particularly in the phase offset estimates. Because the variation in the coherence parameter estimates can exceed acceptable levels,

multiple pulse techniques, as discussed in Section 3.1, or some form of coherence parameter tracking/smoothing should be used. The green curves in Figure 19 show that a simple Kalman coherence filter can be used to significantly reduce the range and phase residuals to provide more reliable coherence parameter estimates.

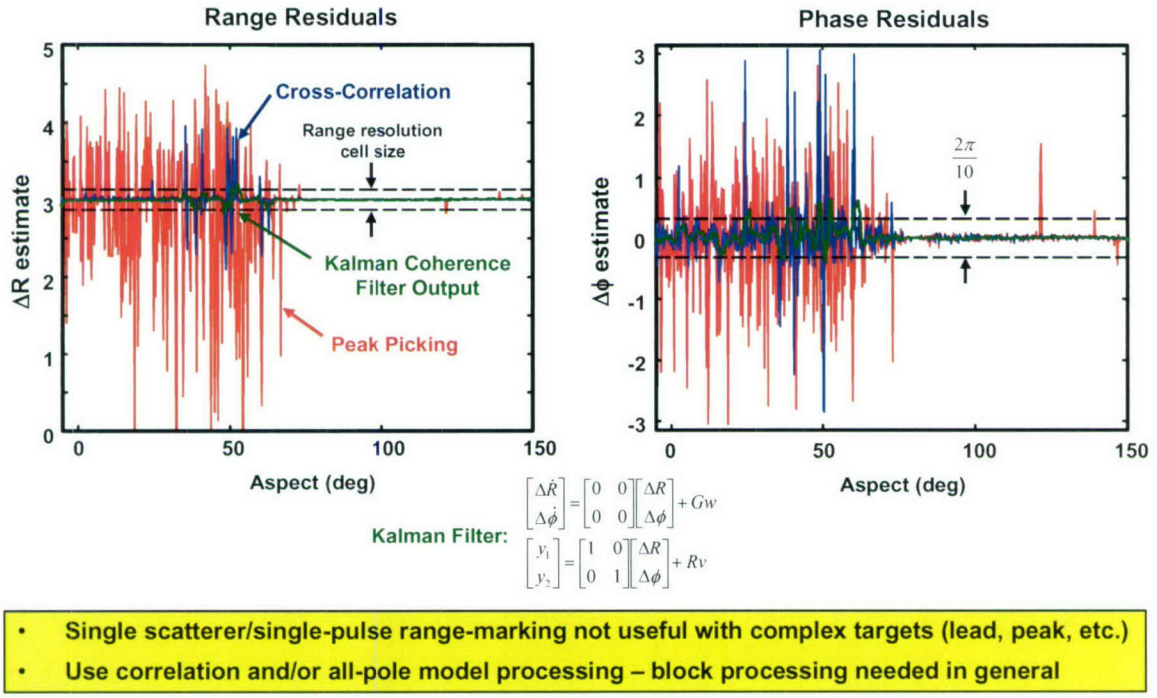

Figure 19. Complex target range and phase residuals from coherence parameter estimation algorithm. Single-pulse, cross-correlation processing with and without Kalman smoothing demonstrated in this example.

Figure 20 shows single and multiple radar RTIs and images. The multi-radar plots use the coherence parameter estimates from the Kalman tracking/smoothing filter shown in Figure 19. By combining the four monostatic and bistatic returns, the NexGen cohered RTI and images show about a 6-dB improvement in SNR relative to the single radar results. This improvement in SNR can be important at certain aspect angles were it is difficult to measure the size, shape, and/or length of the target. This can be seen most clearly by comparing the 45 deg aspect images in Figure 20.

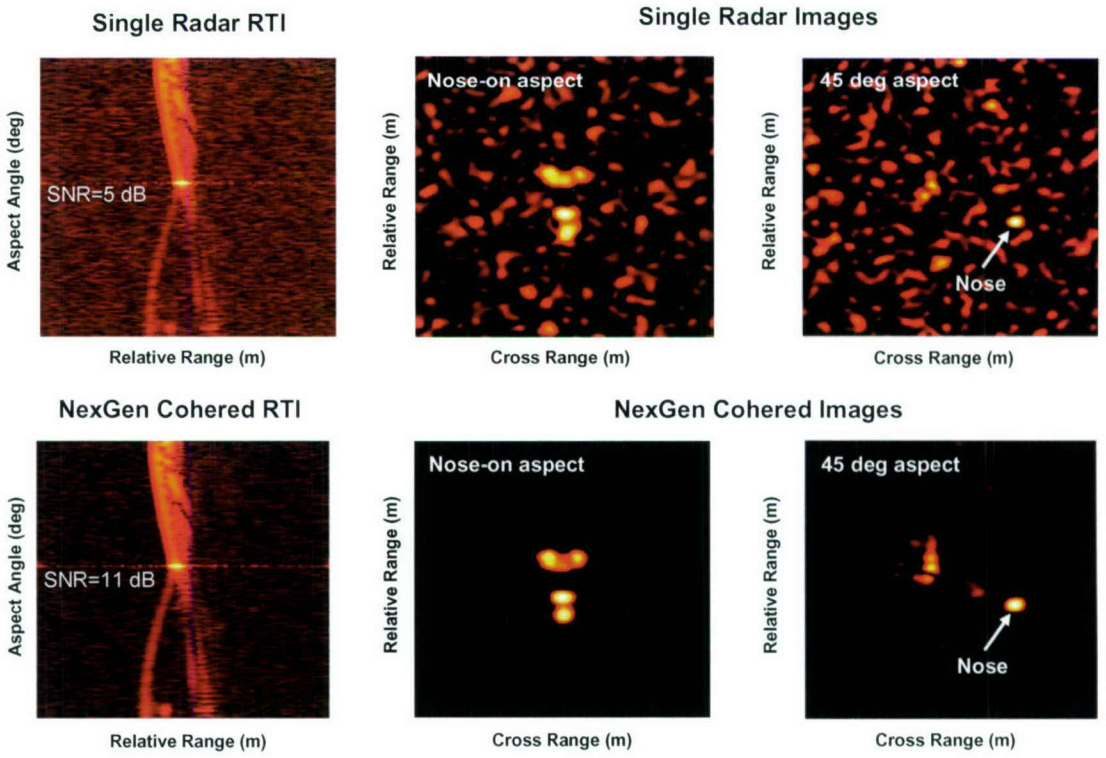

Figure 20. Multi-static cohered data. The NexGen cohered RTI and images show considerable improvements in SNR and target characterization capability.

While these results appear promising, more work needs to be done in order to fully assess coherence parameter estimation and tracking performance over a wider range of SNRs using a variety of realistic targets. In the next section, we compare the computational complexity of the various approaches to radar coherence parameter estimation presented in Section 3.1.

3.4 COMPUTING REQUIREMENTS

Section 3.1 describes six different processing options to adaptively estimate coherence parameters (ΔR and $\Delta\phi$) for N separate radar apertures. Three of these options estimate coherence parameters from a single pulse, while the remaining three estimate coherence parameters from multiple pulses. Recall, we estimate the coherence parameters from multiple pulses when the signal-to-noise ratio from a single radar echo is insufficient for the required level of accuracy. For convenience, Table 1 lists these six processing options.

TABLE 1

Processing Options for Estimating Coherence Parameters

Processing Option	Processing Description	Pulses
1	Peak Pick	Single
2	1D Cross-correlation	Single
3	1D All-pole Modeling	Single
4	Coherent Integration with Cross-correlation	Multiple
5	Coherent Integration with All-pole Modeling	Multiple
6	2D All-pole Modeling	Multiple

Section 2 describes two different processing arrangements, a master-slave arrangement and a cooperative arrangement. Both processing arrangements apply to all of the processing options listed in Table 1. Recall, the master-slave arrangement estimates coherence parameters with the N radar echoes received by the master sensor. The cooperative arrangement estimates coherence parameters from all N^2 radar echoes available in the NGR multi-static radar concept. Section 3.2 shows that in using more radar echoes, the estimates from the cooperative arrangement achieve better performance than the master-slave arrangement. Throughout this section we consider the cooperative arrangement for the NGR field experiments with N=2 apertures and examine the computational requirements for the different processing options listed in Table 1. With N=2, the computational complexity of the master-slave arrangement is approximately half the computational complexity of the cooperative arrangement. This section also specifies the processing hardware required for a real-time implementation on an SGI Origin 3000 multi-processor computer.

3.4.1 Computational Breakdown

In the following we analyze the computational complexity for the six processing options listed in Table 1 from routines implemented in MATLAB. We analyze the major computations in each MATLAB routine to determine the computational cost for each processing option. This analysis utilizes the computational cost in floating point operations for commonly used signal processing kernels documented in [15].

Table 2 defines the data parameters used in our subsequent computational complexity analysis together with an estimate of some typical values for each of these parameters.

TABLE 2

Computational Parameter Definitions

Parameter	Parameter Description	Typical Value
L	Number of samples in the uncompressed pulse	128
K	Number of samples in the compressed pulse	1024
M	Number of cross-correlation lags (for estimating ΔR)	100
n	Hankel parameter for all-pole modeling	L/3
m	Hankel parameter for all-pole modeling	L-n+1
d	Number of target scatterers to estimate	10
P	Number of pulses to coherently integrate	10

Table 3 lists the major operations in the *Peak Pick* processing approach and the associated computational requirements in floating point operations. Note the expressions for the floating point operations in the second column are expressed in terms of the number of samples in the uncompressed pulse, L, and the corresponding number of samples in the compressed pulse, K.

TABLE 3

Computational Requirements for Peak Picking

Description of Major Operations	Floating Point Operations	Line Number(s)
Complex FFT	$4(5L\log_2(L))$	6, 8, 14, 16
Complex IFFT	$4(5K\log_2(K))$	7, 9, 15, 17

Table 4 lists the major operations for the *1D Cross-correlation* processing option. In Table 4 and throughout this section, we assume 50 floating point operations are required to compute a single complex exponential of the form $\exp(j\phi)$. The expressions for floating point operations are expressed in terms of the number of samples in the signal model or uncompressed data vector, L, the number of points used in the FFT-based compressed pulse, K, and the number of range shifts or cross-correlation lag points to consider, M. Most of the operations listed in Table 3 consist of either computing a complex exponential or a matrix-matrix product.

TABLE 4

Computational Requirements for 1D Cross-correlation

Description of Major Operations	Floating Point Operations	Line Number(s)
Undo pulse compression	$20L\log_2(L) + 8L$	2-5
Element multiply for cross-correlation	$12L$	7, 8
FFT for cross-correlation	$10K \log_2(K)$	9, 10
Coherently add cross-correlation	$2K$	11
Normalize cross-correlation	$5K$	12
Least squares fit for interpolated range	72	20
Coarse interpolated range estimate	6	21, 22
Coarse interpolated phase estimate	100	23
Range values for cost function	$M + 4$	24-27
Frequency values for cost function	L	28
Complex exponential	$M(51L)$	32
Element-wise multiply	$M(12L)$	33, 34
Least-squares fit	$M(24L + 1)$	35
Evaluate cost function	$M(28L + 1)$	36
Locate minimum	M	38
Final interpolated range offset	78	40, 41, 44-46
Complex exponential	$51L + 3$	47
Least-squares fit	$12L$	50
Final interpolated phase offset	$24L + 51$	48, 49, 51

The *1D All-pole modeling* processing option consists of all the operations listed for the *1D Cross-correlation* processing option. Table 5 lists the additional major operations required to form one all-pole signal model and the associated computational requirements. Recall that we implement N^2 all-pole models in the cooperative approach, one for each of the N^2 radar echoes. Note that the expressions for the floating point operations in the second column are expressed in terms of the number of samples in the

uncompressed data vector, L, the dimensions of the Hankel matrix used in signal modeling, $m \times n$, and the dimension of the signal space, d. With typical parameter values (L=128, m=86, n=43 and d=10), the floating point operations for the singular value decomposition (SVD) accounts for approximately **96%** of the total computational cost for all-pole signal modeling.

TABLE 5

Additional Computational Requirements for All-pole Signal Modeling

Description of Major Operations	Floating Point Operations	Line Number(s)
SVD without right singular vectors	$16m^2n + 24mn^2$	7
AIC model order estimate	$2n^2 + 60n$	11, 12
Model order estimate	n	14
Matrix multiply	$8d^2n + d$	16
Matrix multiply	$16d^2(n - 1)$	18
Matrix inverse	$8d^2(d - d/3) + 8d^2$	18
Matrix multiply	$8d^3$	18
Eigenvalues	$16/3d^3$	18
Normalize eigenvalues	$10d$	19
Complex multiplies	$6Ld$	22
Matrix multiplies	$8Ld^2 + 8Ld$	24
Matrix inverse	$8d^2(d - d/3) + 8d^2$	24
Matrix multiply	$8Ld^2$	24
Matrix multiply	$8Ld$	25

Coherent Integration with 1D Cross-correlation consists of first coherently combining multiple pulses followed the same 1D Cross-correlation operations listed in Table 4. Table 6 lists the additional major operations required for coherent integration which consists of complex exponentials, complex multiplications and complex additions. In the table, the variable P refers to the number of pulses coherently integrated. We envision coherent integration with approximately ten pulses. Note, the operations in Table 6 are repeated four times with N = 2 in the cooperative arrangement.

TABLE 6

Additional Computations for Coherent Integration with 1D Cross-correlation

Description of Major Operations	Floating Point Operations	Line Number(s)
Complex exponential	$52PL + P + L$	3
Complex multiply and addition	$6PL + 2(P\text{-}1)L$	4

Similar to Coherent Integration with 1D Cross-correlation, *Coherent Integration with 1D All-pole Modeling* consists of first performing the operations listed in Table 6 followed by the operations listed in Tables 4 and 5. The operations required for coherent integration turn out to be minimal.

The *2D All-pole Modeling* processing option is a two-dimensional extension of the 1D All-pole Modeling processing option. As such, the computational requirements are also dominated by the SVD operation. Recall that the computational requirements for a complex SVD in Table 5 was listed as $16m^2n + 24mn^2$ real floating point operations where m and n are the dimensions of the Hankel matrix. The 2D All-pole Modeling operation performs a complex SVD on a large block Hankel matrix. With $P = 10$ pulses, the dimensions of the block Hankel matrix are typically $5m \times 5n$. Consequently, a large percentage of the computational cost for the 2D All-pole modeling operation is approximately $2{,}000m^2n + 3{,}000mn^2$ real floating point operations.

3.4.2 Processing Requirements

In this section, we use the expressions from the previous section to compute the sustained processing throughput required for the different processing options. Table 7 lists the processing requirements for the six different processing options assuming the following parameter values: K=1024, L=128, M=100, d=10, m=86, n=43 and P=10. The third column in Table 7 is labeled "Sustained Throughput" and represents the total number of million floating point operations per second (MFLOPS) required for a 10 Hz update rate. Recall that the computations in the all-pole modeling operation are dominated by a matrix SVD. Unfortunately, SVDs exhibit inefficient implementations on general purpose programmable processors. Typically only 10% processing efficiency is achieved [16]. In contrast, most of the other operations are dominated by complex multiples and complex sums which can be rather efficient on general purpose programmable hardware. We estimate 40% processing efficiency for operations other than SVDs. The fourth column in Table 7 is labeled "Required Peak Throughput" and represents the real-time processor requirements for each operation assuming the estimated processing efficiencies and a 10 Hz update rate.

TABLE 7

Processing Requirements for Different Processing Options

Processing Option	Processing Description	Sustained Throughput (MFLOPS) *	Required Peak Throughput (MFLOPS) *	Max. Update Rate (Hz) **
1	Peak Pick	2.2	5.6	>100
2	1D Cross-correlation	16	41	>100
3	1D All-pole Modeling	390	3,700	7.2
4	Multipulse Integration/Cross-correlation	21	52	>100
5	Multipulse Integration/All-pole Modeling	390	3,800	7.2
6	2D All-pole Modeling	~45,000	~450,000	.016

* 10 Hz update rate

** 700 MHz MIPS processor(s) with 50% spare computational resources

Table 7 indicates that the computational load is minimal for processing options 1, 2, 4 and 5. In fact, with modern computing technology, the required peak throughput for these processing options is computationally insignificant. However, the processing options that implement all-pole modeling (processing options 3, 6 and 7) have more stringent computational requirements. Recall the cooperative approach for processing options 3 and 6 implement four separate all-pole modeling operations. Since the all-pole modeling operations are independent of one another, they may be performed in parallel on separate processors. Furthermore, if we assume the parameter values listed earlier then the peak throughput requirement for a single all-pole modeling operation is approximately 930 MFLOPS. The computational requirement for the current 2D all-pole modeling algorithm is large, but work is underway to make this algorithm much more computationally tractable. Consequently, this option is not necessarily out of reach of current programmable computing hardware.

Let us assume that the NGR field experiments will be conducted with the MPS-36s at the Reagan Test Site (RTS). After the ROSA upgrades, each MPS-36 will include an SGI Origin 3000-class main computer. A relatively simple and inexpensive processing solution for real-time coherence parameter estimation is to add more processing nodes to the main computer (the Origin 3000 has a scalable design which can accommodate up to 128 MIPS processors). Each MIPS processor is equipped with two

independent floating point units. Therefore, the R14000A MIPS processor operating at a 600 MHz clock speed has a theoretical peak performance of 1,200 MFLOPS. Similarly, the R16000 MIPS processor operating at a 700 MHz clock speed is theoretically capable of 1,400 MFLOPS. For either processor, the theoretical peak processing capabilities is not much greater than the required peak throughput requirements for the all-pole modeling operation (930 MFLOPS). Note that to minimize risk, we generally require that the processor capabilities be at least twice the peak processing requirement, which implies a processor whose capabilities are at least 1,860 MFLOPS .

If all-pole modeling is required, then we recommend two alternatives to mitigate the processing risk in the all-pole modeling operation. The first is to benchmark the SVD operation on the MIPS processor. The benchmarks should be performed with different matrix dimensions including the 86×43 dimension matrices considered here. If the processing efficiency for the SVD operation on the MIPS processor is low, as predicted here, we have a second recommendation. We recommend reducing the number of samples in the signal model or data vector, L. For example, if L is reduced from 128 to 96 then the dimension of the matrix for the SVD operation is reduced from 86×43 to 65×32. These reduced parameter values reduce the peak throughput requirements for the all-pole modeling operation from 930 MFLOPS to 400 MFLOPS. This reduced processing requirement is less than half of the peak processing capabilities of either the R14000A or R16000 MIPS processors. In this case, the entire all-pole modeling operation can be performed on a single MIPS processor at low risk in the allotted time (0.10 second).

Based on the MIPS processor capabilities, Table 7 indicates that processing options 1, 2, and 4 require only a fraction of the capabilities of a single MIPS processor at a 10 Hz update rate. Furthermore, the processing requirements for processing options 3 and 5 indicate that four MIPS processors are required for a 10 Hz update rate with the cooperative arrangement and two MIPS processors with the master-slave arrangement. Another way of viewing the real time performance of these different processing options is listed in the last column of Table 7. We assume that a single 700 MHz MIPS processor is used to implement processing options 1, 2, and 4 and we assume that four MIPS processors are used to implement processing options 3 and 5. In the last column of Table 7, we list the maximum update rate that can be supported for each processing option. Processing options 1, 2, and 4 can be updated in excess of 100 Hz while processing options 3 and 5 can only be updates on the order of 7 Hz. As indicated earlier we recommend benchmarking the SVD operation on the MIPS processor to verify these predictions.

4. CONCLUSIONS AND RECOMMENDATIONS

4.1 CONCLUSIONS

In this report, we have presented robust signal processing architectures and algorithms specifically designed to achieve multi-aperture coherence on transmit and receive. By transmitting orthogonal radar waveforms, the monostatic and bistatic target returns can be separated at each receiver's matched filter output. These returns can then be analyzed to determine the appropriate transmit times and phases in order to cohere the various radar apertures. This provides an adaptive closed-loop process for cohering the radar apertures and for periodically monitoring mutually coherent operation. Our use of orthogonal waveforms increases the array gain to N^2 instead of N for the single transmitter case. Furthermore, when full coherence on transmit is achieved, the gain is N^3.

The performance of our coherence algorithms were quantified using Monte Carlo simulations and compared to the Cramer-Rao lower bound. Best performance is achieved with the cooperative radar architecture, i.e. when all N^2 return signals available at the receivers are used to estimate the required target coherence parameters. Target range marking and phase estimation is best achieved by cross-correlating the multi-static target return signals. This approach uses the target's full range response and, in general, outperforms other methods when the target consists of many scattering centers. It was also shown that all-pole signal modeling is useful for removing some of noise from the target returns prior to correlation processing. Consequently, this approach appears to work better than standard correlation processing when the target is complex and/or the data is very noisy.

A computational complexity study showed that our aperture coherence algorithms are suitable for a real-time implementation on an SGI Origin 3000 multi-processor computer. It was also shown that a single 700 MHz MIPS processor is capable of providing a 100 Hz coherence parameter update rate when standard cross-correlation processing is used. Four of these processors are required for all-pole modeling to achieve a coherence parameter update rate of about 7 Hz.

4.2 RECOMMENDATIONS

Based upon a preliminary investigation of several candidate aperture coherence algorithms, the following general recommendations can be made for initial field experiments.

1. Implement the cooperative-radar signal processing architecture. This architecture uses all N^2 return signals available at the receivers to estimate the required target coherence parameters.

2. Estimate the target coherence parameters by cross-correlating the multi-static target return signals. This approach uses the target's full wideband range response and is expected to

outperform other methods, such as peak-picking or centroid, when the target consists of many competing scattering centers.

3. Consider using all-pole signal modeling techniques to "clean up" the target return signals for targets at very low SNR levels and/or when buried in heavy clutter.

There are also a number of important signal processing efforts still needed. Some of these efforts are listed below.

- Multi-static Doppler (velocity) updating vs. Performance. When multi-radar apertures are widely spaced, target induced Doppler effects become increasingly important.

- Only an elementary attempt has been made in this report to integrate the fine range and phase measurements over time. This is an important area of future effort as it would allow for some level of coherence parameter prediction into the future, i.e. pulses up to time t_i are used to estimate the target coherence parameters and these parameters could then be adjusted to accommodate transmitted pulses at time t_{i+1}, etc.

- Resistance of our algorithms to electronic counter measures (ECM) is also important. Specifically, the use of broadband noise waveforms and 2D all-pole models to help mitigate severe clutter/jammer noise needs to be more formally investigated.

REFERENCES

1. K.M. Cuomo, and J.E. Piou, and J.T. Mayhan, "Ultra-Wideband Coherent Processing," *The Lincoln Laboratory Journal*, **10**, 2, 203-222, 1997.

2. K.M. Cuomo, and J.E. Piou, and J.T. Mayhan, "Ultra-Wideband Coherent Processing," *IEEE Trans. Ant. & Prop.*, **47**, 6, 1094-1107, June 1999.

3. J.T. Mayhan, M.L. Burrows, K.M. Cuomo, and J.E. Piou, "High Resolution 3-D 'Snapshots' ISAR Imaging and Feature Extraction," *IEEE Trans. Aerosp. Electron. Sys.*, **37**, 630-642, April 2001.

4. J.E. Piou, K.M. Cuomo, and J.T. Mayhan, "A State-Space Technique for Ultrawide-Bandwidth Coherent Processing," MIT Lincoln Laboratory, Lexington, Mass., Technical Report 1054, 20 July 1999, DTIC ESC-TR-98-066.

5. G.W. Ahlgren – Editor, "Next Generation Radar Concept Definition Team Final Report," June 2003.

6. M.I. Skolnik, D.I. King, "Self-Phasing Array Antennas", IEEE Transactions on Antennas and Propagation, AP-12, March 1964.

7. J.H. Schrader, "Receiving System Design for the Arraying of Independent Steerable Antennas, IEEE Transactions on Antennas and Propagation, AP-12, March 1964.

8. J.W. Eberle, An Adaptively Phased, Four-Element Array of Thirty-Foot Parabolic Reflectors for Passive (Echo) Communication Systems, IEEE Transactions on Antennas and Propagation, AP-12, March 1964.

9. F.C. Robey, M. Belcher, M. Budge, K. Nash, J. Frank, A.S. Fletcher, "Next Generation Radar Study Results," MIT Lincoln Laboratory, February 2003.

10. E.D. Sharp and M.A. Diab, "Van Atta Reflector Array, IRE Transactions on Antennas and Propagation, vol. AP-8, July 1960.

11. S.T. Smith, "Accuracy and Resolution Bounds for Adaptive Sensor Array Processing," 9th IEEE Worksop on Statistical Signal Array Processing, pp 37-40, September 1998.

12. J.E. Piou, K.M. Cuomo, and J.T. Mayhan, "A State-Space Technique for Ultrawide-Bandwidth Coherent Processing," MIT Lincoln Laboratory, Lexington, Mass., Technical Report 1054, 20 July 1999, DTIC ESC-TR-98-066.

13. A.W. Rihachek, Principles of High-Resolution Radar, MARK Resources, Inc., 1977.

14. A.S. Fletcher and F.C. Robey, "Performance Bounds for Adaptive Coherence of Sparse Array Radar," Adaptive Array Processing Workshop, MIT Lincoln Laboratory, Lexington, March 2003.

15. M. Arakawa, "Computational Workloads for Commonly Used Signal Processing Kernels," *MIT Lincoln Laboratory Project Report SPR-9,* May 2003.

16. J. Lebak, Private Communication, July 2003.

REPORT DOCUMENTATION PAGE

Form Approved OMB No. 0704-0188

Public reporting burden for this collection of information is estimated to average 1 hour per response, including the time for reviewing instructions, searching existing data sources, gathering and maintaining the data needed, and completing and reviewing this collection of information. Send comments regarding this burden estimate or any other aspect of this collection of information, including suggestions for reducing this burden to Department of Defense, Washington Headquarters Services, Directorate for Information Operations and Reports (0704-0188), 1215 Jefferson Davis Highway, Suite 1204, Arlington, VA 22202-4302. Respondents should be aware that notwithstanding any other provision of law, no person shall be subject to any penalty for failing to comply with a collection of information if it does not display a currently valid OMB control number. **PLEASE DO NOT RETURN YOUR FORM TO THE ABOVE ADDRESS.**

1. REPORT DATE *(DD-MM-YYYY)*	2. REPORT TYPE	3. DATES COVERED *(From - To)*
30 July 2004		

4. TITLE AND SUBTITLE
Wideband Aperture Coherence Processing for Next Generation Radar (NexGen)

5a. CONTRACT NUMBER
F19628-00-C-0002

5b. GRANT NUMBER

5c. PROGRAM ELEMENT NUMBER

6. AUTHOR(S)
K.M. Cuomo, S.D. Coutts, J.C. McHarg, N.B. Pulsone, F.C. Robey

5d. PROJECT NUMBER

5e. TASK NUMBER

5f. WORK UNIT NUMBER

7. PERFORMING ORGANIZATION NAME(S) AND ADDRESS(ES)

MIT Lincoln Laboratory
244 Wood Street
Lexington, MA 02420-9108

8. PERFORMING ORGANIZATION REPORT NUMBER
Project Report NG-3

9. SPONSORING / MONITORING AGENCY NAME(S) AND ADDRESS(ES)
Missile Defense Agency
7100 Defense Pentagon
Federal Office Bldg #2
Washington, D.C. 20301-7100

10. SPONSOR/MONITOR'S ACRONYM(S)
MDA/AS

11. SPONSOR/MONITOR'S REPORT NUMBER(S)
ESC-TR-2004-087

12. DISTRIBUTION / AVAILABILITY STATEMENT
Prepared for the Missile Defense Agency under Air Force Contract F19628-00-C-0002.

Approved for public release; distribution is unlimited.

13. SUPPLEMENTARY NOTES

14. ABSTRACT

This report develops robust signal processing architectures and algorithms specifically designed to achieve multi-aperture coherence on transmit and receive. A key feature of our approach is the use of orthogonal radar waveforms that allow the monostatic and bistatic target returns to be separated at each receiver's matched filter output. By analyzing these returns, we may determine the appropriate transmit times and phases in order to cohere the various radar apertures using both narrowband and wideband waveforms. This process increases the array gain on receive to N2 instead of N for the single transmitter case. Furthermore, when full coherence on transmit is achieved, the array gain is N3. The performance of our coherence algorithms is quantified using Monte Carlo simulations and compared to the Cramer-Rao lower bound. A computational complexity study shows that our aperture coherence algorithms are suitable for a real-time implementation on an SGI Origin 3000 multi-processor computer.

15. SUBJECT TERMS

16. SECURITY CLASSIFICATION OF:			17. LIMITATION OF ABSTRACT	18. NUMBER OF PAGES	19a. NAME OF RESPONSIBLE PERSON
a. REPORT	b. ABSTRACT	c. THIS PAGE	NONE	58	19b. TELEPHONE NUMBER *(include area code)*
U	U	U			